◆ Human Brain Mapping 38:5356–5374 (2017) ◆

Dynamic Coupling between fMRI Local Connectivity and Interictal EEG in Focal Epilepsy: A Wavelet Analysis Approach

Amir Omidvarnia,[1]* Mangor Pedersen,[1] David N. Vaughan,[1,2] Jennifer M. Walz,[1] David F. Abbott,[1] Andrew Zalesky,[3,4] and Graeme D. Jackson[1,2]

[1]*The Florey Institute of Neuroscience and Mental Health and The University of Melbourne, Austin Campus, Heidelberg, Victoria, Australia*
[2]*Department of Neurology, Austin Health, Heidelberg, Victoria, Australia*
[3]*Department of Psychiatry, Melbourne Neuropsychiatry Centre, The University of Melbourne and Melbourne Health, Carlton, Victoria, Australia*
[4]*Melbourne School of Engineering, Building 173, The University of Melbourne, Parkville, Victoria, Australia*

Abstract: Simultaneous scalp EEG-fMRI recording is a noninvasive neuroimaging technique for combining electrophysiological and hemodynamic aspects of brain function. Despite the time-varying nature of both measurements, their relationship is usually considered as time-invariant. The aim of this study was to detect direct associations between scalp-recorded EEG and regional changes of hemodynamic brain connectivity in focal epilepsy through a time-frequency paradigm. To do so, we developed a voxel-wise framework that analyses wavelet coherence between dynamic regional phase synchrony (DRePS, calculated from fMRI) and band amplitude fluctuation (BAF) of a target EEG electrode with dominant interictal epileptiform discharges (IEDs). As a proof of concept, we applied this framework to seven patients with focal epilepsy. The analysis produced patient-specific spatial maps of DRePS-BAF coupling, which highlight regions with a strong link between EEG power and local fMRI connectivity. Although we observed DRePS-BAF coupling proximate to the suspected seizure onset zone in some patients, our results suggest that DRePS-BAF is more likely to identify wider 'epileptic networks'. We also compared DRePS-BAF with standard EEG-fMRI analysis based on general linear modelling (GLM). There was, in general, little overlap between the DRePS-BAF maps and GLM maps. However, in some subjects the spatial clusters revealed by these two analyses appeared to be adjacent, particularly in medial posterior cortices. Our findings suggest that (1) there is a strong time-varying relationship between local fMRI connectivity and interictal EEG power in focal epilepsy, and (2) that DRePS-BAF reflect different aspects of epileptic

Disclosures The authors have no conflicts of interest to disclose.
Contract grant sponsor: National Health and Medical Research Council (NHMRC) of Australia; Contract grant number: 628952; Contract grant sponsor: State Government of Victoria, Australia (Operational Infrastructure Support Grant to The Florey Institute of Neuroscience and Mental Health); Contract grant sponsor: NHMRC (practitioner's fellowship to G.D.J.); Contract grant number: 1060312; Contract grant sponsor: NHMRC postgraduate scholarship and a Windermere Foundation doctoral scholarship (to D.N.V.); Contract grant sponsor: Australian National Imaging Facility (fellowship funding for D.F.A.)

*Correspondence to: Amir Omidvarnia, The Florey Institute of Neuroscience and Mental Health, Melbourne Brain Centre, Austin Campus, 245 Burgundy Street, Heidelberg, Victoria 3084, Australia. E-mail: a.omidvarnia@brain.org.au

Received for publication 2 September 2016; Revised 1 June 2017; Accepted 27 June 2017.

DOI: 10.1002/hbm.23723
Published online 24 July 2017 in Wiley Online Library (wileyonlinelibrary.com).

network activity than standard EEG-fMRI analysis. These two techniques, therefore, appear to be complementary. *Hum Brain Mapp 38:5356–5374, 2017.*

Key words: simultaneous EEG-fMRI; functional connectivity; wavelet coherence; DRePS; focal epilepsy

INTRODUCTION

Integration of scalp electroencephalogram (EEG) and its concurrent blood oxygenation level dependent (BOLD) changes encoded in functional MRI (fMRI) data is a widely used approach for studying brain function. This is mainly because EEG provides temporally rich information about brain dynamics, whilst fMRI offers millimetre spatial resolution about engaged brain regions. Simultaneous acquisition of EEG and fMRI is particularly useful in focal epilepsy studies, where EEG conveys the times at which epileptiform activity is present and fMRI maps its spatial location [Allen et al., 1998; Fahoum et al., 2012, 2013; Flanagan et al., 2014; Laufs et al., 2007, 2011; Masterton et al., 2013; Mulert and Lemieux, 2010]. In most simultaneously acquired EEG-fMRI data analyses in focal epilepsy studies, the only information from the EEG that is used to generate the result is the timing of the interictal epileptiform discharges (IEDs). It is therefore desirable to develop EEG-fMRI data fusion methods that better exploit mutual aspects of EEG and fMRI in impaired brain function including focal epilepsy.

Focal epilepsy is a neurological disease with symptoms that partly depend on the anatomical location of the epileptogenic foci [Noachtar and Peters, 2009]. This disease can compromise the configuration of functional brain networks beyond the seizure onset zones [Berg et al., 2010; Federico et al., 2005; Gotman, 2008; Iannotti et al., 2016; Pedersen et al., 2015]. Clinically, epileptic brain regions and networks are identified through comprehensive assessment of the electroclinical syndrome and the patient's multimodal brain imaging data. An important marker of focal epilepsy is the existence of IEDs in the scalp EEG. These result from synchronous neuronal firing across at least 10–20 cm^2 of the cortex [Tao et al., 2007]. IEDs are associated with increases in cerebral glucose metabolism and blood flow [Bittar et al., 1999] which, in turn, can affect the properties of simultaneously acquired EEG spectral power [Kilner et al., 2005]. Conversely, fMRI signals are likely dominated by metabolic changes related to synaptic currents and action potential propagation [Attwell and Laughlin, 2001]. This suggests that the instantaneous power envelope (also called band amplitude fluctuation or BAF [Tokariev et al., 2012]) of scalp interictal EEG and fMRI signals may share mutual aspects of brain function in focal epilepsy.

Increased segregation (i.e., abnormally increased 'local connectivity') of functional nodes in resting-state epileptogenic networks is another feature of focal epilepsy that is seen in both EEG and fMRI studies [Pedersen et al., 2016; Ponten et al., 2007; Schindler et al., 2008]. In order to quantify local functional connectivity changes in focal epilepsy, Regional Homogeneity (ReHo) has been previously employed [Pedersen et al., 2016]. Combined Fluorodeoxyglucose positron emission tomography (FDG-PET) and MR studies have revealed mutual relationships between ReHo maps and PET images suggesting a coupling between brain metabolism and local functional connectivity [Aiello et al., 2015]. An assumption of ReHo is that the brain's functional networks remain static over time [Zang et al., 2004]. However, there is increasing evidence that dynamics of brain functional connectivity during resting-state periods are time-varying [Chang and Glover, 2010; Tailby et al., 2015; Zalesky et al., 2014]. To address this point, a Dynamic Regional Phase Synchrony (DRePS) measure has been developed as a time-varying version of ReHo with similar temporal resolution to the input fMRI time series [Omidvarnia et al., 2016]. This method has recently been applied to detect changes in the dynamics of functional connections in neocortical focal epilepsy [Pedersen et al., 2017].

In the present study, we quantitatively investigate the relationship between simultaneously acquired EEG and fMRI data in focal epilepsy from the perspective of brain functional connectivity. In seven patients with frontal and/or temporal lobe epilepsy, we study time-varying behaviour of local network properties using a DRePS-BAF coupling approach that is based on wavelet coherence analysis. This method detects scale-dependent similarities between power envelopes of an EEG channel with dominant IEDs and fluctuations of local dynamic functional connectivity quantified by DRePS. We hypothesise that such an analysis will be complementary to conventional general linear modeling (GLM) analysis of interictal events in simultaneous EEG-fMRI, with each method revealing somewhat different aspects of epileptic networks.

MATERIALS AND METHODS

Overview of DRePS-BAF Coupling: A Proposed Data Fusion Method

The proposed multi-step DRePS-BAF coupling analysis can be summarized as follows (see also Fig. 1):

A. Dynamic local connectivity information of the fMRI data is extracted through DRePS analysis. It results in a 4D map with the same temporal resolution as the fMRI data. See Step A: Extraction of dynamic local fMRI connectivity using DRePS section for more details.

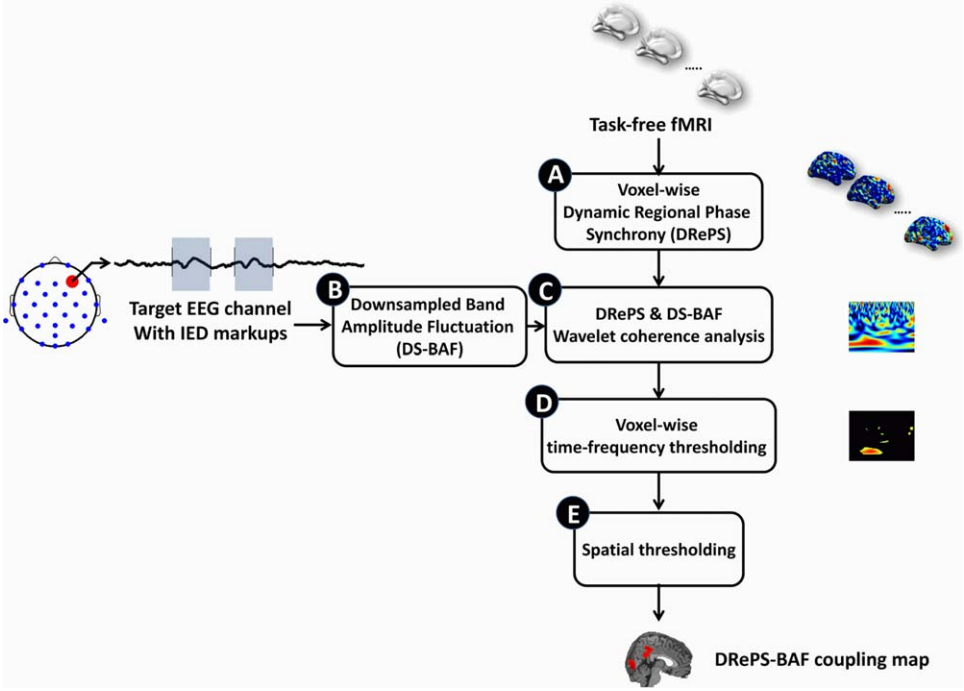

Figure 1.

Block diagram of the proposed DRePS-BAF coupling analysis approach. See Overview of DRePS-BAF coupling: a proposed data fusion method section for description of the blocks. [Color figure can be viewed at wileyonlinelibrary.com]

B. A target EEG electrode is selected where the dominant IED events occur (i.e., the greatest mean IED amplitude over all electrodes). The downsampled band amplitude fluctuation (DS-BAF) of this target channel is computed at the same sampling frequency as the fMRI. This achieves a match between the temporal resolution of the EEG and the fMRI time series. See Step B: Downsampled band amplitude fluctuation section for more details.

C. A voxel-wise Morlet wavelet coherence analysis is performed between the DS-BAF of the target EEG channel and the DRePS time series. It leads to a 2D wavelet

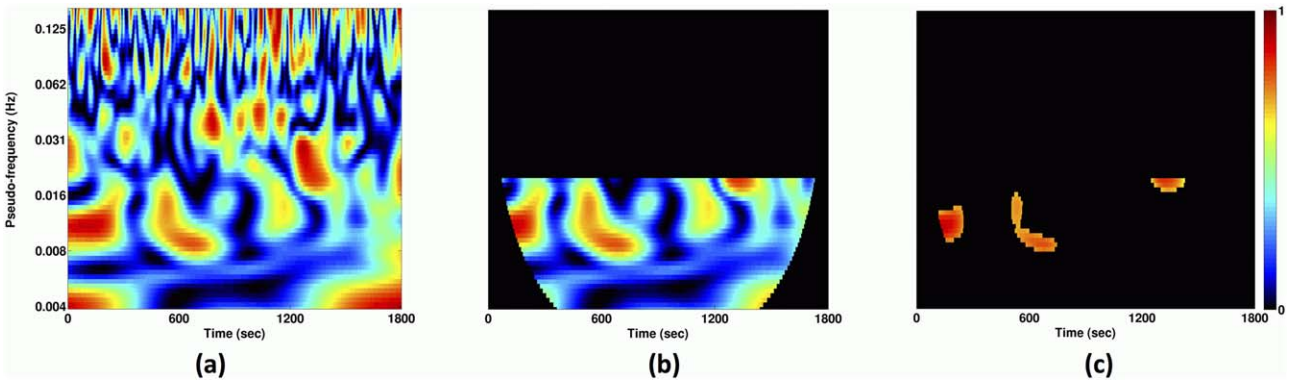

Figure 2.

(a) Example of a DRePS-BAF wavelet coherence map, (b) its values within a desired frequency interval avoiding the 'cone of influence' where wavelet edge effects become pronounced and (c) its thresholded version at the 95th percentile which consists of features we denote as 'T-F patches' for a typical voxel. A 'T-F patch size ratio' is then defined for each voxel as the sum of T-F values within patches divided by the sum of entire values outside the cone of influence and within the desired frequency band. [Color figure can be viewed at wileyonlinelibrary.com]

coherence plane for each voxel (an example can be seen in Fig. 2a). See Step C: Analysis of DRePS-BAF coupling using Morlet wavelet coherence section for more details.

D. Each voxel-wise wavelet coherence map is thresholded at a certain percentile (here, 95th) of the distribution of values outside its cone of influence and within a desired frequency band (an example can be seen in Fig. 2b). It leads to a sparse 2D binary map with a few time-frequency (T-F) patches, within which similarity between DRePS and DS-BAF is greatest (Fig. 2c). From this point onwards, we refer to this EEG-fMRI relationship as 'DRePS-BAF coupling'.

E. A 'T-F patch size ratio' is then defined for each voxel as the sum of T-F values within patches divided by the sum of entire values outside the cone of influence and within the desired frequency band (Fig. 2b). T-F patch size ratios at all voxels form a 3D *DRePS-BAF coupling map* in which non-zero voxels show the strongest time-frequency link between the downsampled power envelope of the target EEG electrode and dynamic local functional connectivity. The frequency interval of the EEG power envelope is estimated with reference to the IED markup. See Step B: Downsampled band amplitude fluctuation and Steps D–E: Time-frequency thresholding and T-F patch ratio analysis sections for more details.

Figure 1 illustrates a block diagram of the proposed approach regarding the above labelling.

Participants and Simultaneous EEG-fMRI Scanning Procedure

We studied datasets of temporal, frontal, or temporo-frontal lobe epilepsy patients who had EEG-fMRI recordings performed at the Florey Institute and Neuroscience and Mental Health (Melbourne, Australia) over the last 3 years for surgical consideration. Our inclusion criteria were:

a. At least 30 min of simultaneous EEG-fMRI recording with no interruption such as the occurrence of a seizure,
b. Acceptable EEG quality, after magnetic field gradient and motion artefact correction, to confidently identify IEDs,
c. At least 20 focal IEDs throughout the length of the dataset.

Of more than 20 available datasets, 7 met inclusion criteria and were used in the following analysis. It is important to note that combined EEG-fMRI studies are particularly difficult in well-characterized electroclinical syndromes such as mesial temporal lobe epilepsy and hippocampal sclerosis because IEDs are often very infrequent. Instead we studied patients with focal epilepsy who did have frequent IEDs.

All patients were scanned with a 3T Siemens Skyra MRI system (Erlangen, Germany). Functional data were acquired using an echo-planar imaging (EPI) sequence with 44 interleaved 3 mm-thick slices, $T_R = 3$ s, $T_E = 30$ ms, flip angle = 85°, voxel size of $3 \times 3 \times 3$ mm and an acquisition matrix of 72×72. A total of 600 volumes (30 min) of resting-state fMRI data were used for all patients. T_1-weighted images were also acquired following the functional scans.

Simultaneous EEG data were acquired using a 32-channel MR-compatible EEG cap (BrainCap MR, EasyCap GmbH, Breitbrunn, Germany) according to the 10–20 standard system. All patients were instructed to close their eyes and fall asleep, as this may increase the probability of IED occurrence during EEG recording. Data were recorded based on the Referential montage at the sampling rate of 5,000 Hz with reference to the FCz electrode, but further converted to average reference. Multichannel EEG recording of each patient was marked for IED events by an EEG expert according to recommended guidelines [Flanagan et al., 2009]. For each subject in our cohort, we chose the most frequent type of epileptogenic discharge (i.e., focal spikes for all subjects). We noticed other types of epileptogenic discharges on EEG recordings in some patients, but their number was considerably lower than focal spikes and insufficient for our analyses. The IEDs of interest were then averaged for each EEG channel, and the channel associated with the largest mean IED amplitude in that patient was chosen as the target channel (e.g., the electrode T7 for Patient 1 in Fig. 5a). Target EEG electrodes are listed for all patients in Table I. The study was approved by the Austin Health Human Research Ethics Committee and all patients gave written consent to participate in the study.

We have previously used EEG and fMRI datasets of 6/7 patients (all except for Patient 6) in an unrelated study [Walz et al., 2017]. However, preprocessing of EEG and fMRI data, total data length and statistical analyses vary between our two studies.

EEG-fMRI Data Preprocessing

All fMRI data were preprocessed in MATLAB (MathWorks Inc., Natick, MA) using Statistical Parametric Mapping (SPM8, Welcome Department of Imaging Neuroscience, Institute of Neurology, London) and DPABI [Yan et al., 2016] toolboxes. fMRI preprocessing steps included: slice timing correction and re-alignment of the EPI images for head motion correction, segmentation of T_1-weighted images into white matter, grey matter and cerebrospinal fluid areas using SPM8, coregistration of EPI images to the patient's own T_1-weighted images and finally, spatial normalization to the standard MNI[1] space (152-brain average template).

[1]Montreal Neurological Institute.

TABLE I. Clinical details of participants

Patient	Gender	Age	Age of seizure onset	Epilepsy type	Target EEG electrode	No. of events	Clinical findings
1	M	42	10y	Left TLE	T7	99	Tuberous sclerosis at inferior surface of left temporal lobe, 4.5 cm from temporal pole (MRI), left temporal hypo-metabolism (PET), left temporal hyper-perfusion (iSPECT)
2	F	42	7y	Left TLE	T7	238	Periventricular nodular heterotopia (MRI): heterotopic grey matter nodules in temporal horn of left ventricle and left temporal lobe, and overlying temporal neocortex
3	F	29	16y	Left TLE or multifocal	T7	274	Suspected abnormality at left anterior temporal lobe and hippocampus (MRI), left anterior temporal hypo-metabolism (PET), left temporal hyper-perfusion (iSPECT)
4	F	40	3mo	Right FLE or multifocal	Fz	31	Multiple right frontal locations suspicious for bottom of sulcus dysplasia (MRI), right superior frontal hypo-metabolism (PET) and hyper-perfusion (iSPECT)
5	M	41	16y	Bilateral TLE	T7	140	Ongoing seizure after right anterior temporal lobectomy, suspected structural abnormality at inferior right posterior temporal regions (MRI), right temporal hypo-metabolism and left temporal hyper-metabolism (PET), right frontal and posterior temporal hyper-perfusion (iSPECT)
6	M	26	13y	Right FLE	Fp2	46	Suspected abnormality at right frontocentral regions (MRI), left frontal hypo-metabolism (PET), hyper-perfusion to the right temporal, mesial frontal and right frontal polar cortex (iSPECT)
7	F	28	8y	Right TLE	T8	21	Suspected abnormality at right posterior temporal lobe (MRI), right posterior temporal hypo-metabolism (PET) and hypo-perfusion (iSPECT)

Abbreviations: M = male, F = female, y = year, mo = month, TLE = temporal lobe epilepsy, FLE = frontal lobe epilepsy, MRI = magnetic resonance imaging (structural), PET = positron emission tomography, iSPECT = ictal single photon emission computed tomography.

For DRePS analysis, the spatially normalized images were not smoothed as smoothing can introduce spurious connectivity between neighbouring fMRI voxels. Average white matter and cerebrospinal fluid signals as well as 6 motion parameters were regressed out from the data. Image volumes with excessive head movement (framewise displacement >0.5 mm [Power et al., 2012]) were omitted and replaced using cubic spline interpolation. Finally, BOLD data were bandpass filtered within the ranges of 0.03–0.07 Hz in preparation for DRePS analysis [Omidvarnia et al., 2016].

For standard (GLM) EEG-fMRI analysis, slice time corrected and spatially normalized datasets were smoothed using a spatial Gaussian filter with full-with at half maximum (FWHM) of 8 mm.

EEG signals were preprocessed using the Brain Vision Analyser software (version 2.0, Brain Products) and the EEGLAB toolbox [Delorme and Makeig, 2004]. Gradient-switching artifacts were corrected by subtracting the averaged scanner artifact template from the continuous EEG recordings using the information of scanner markups [Allen et al., 2000]. The preprocessed EEG signals were further downsampled to 250 Hz. Cardioballistic artifacts were corrected automatically using information obtained via motion artefact detection loops [Abbott et al., 2015; Masterton et al., 2007].

Step A: Extraction of Dynamic Local fMRI Connectivity Using DRePS

DRePS is a measure of dynamic local functional connectivity, based on time-varying mean phase coherence among neighbouring voxels in resting-state fMRI data [Omidvarnia et al., 2016]. It reflects locally synchronous hemodynamic changes and is likely to be an indicative of time-varying metabolic cost of brain regions.

Let $\varphi_x[n]$ and $\varphi_{y_i}[n]$ be the instantaneous phase (IP) functions of the bandpass filtered fMRI time series $x[n]$ and $y_i[n]$ consisting of T volumes ($n=1,\ldots,T$) at a given voxel x and its neighboring voxels y_i ($i=1,\ldots,M-1$) where M is the entire number of non-zero voxels within a $3 \times 3 \times 3$ voxel moving cube (including voxel x). The IPs are obtained from $z_x[n]$ and $z_{y_i}[n]$, that is, the analytic associates of $x[n]$ and $y_i[n]$, respectively, using the Hilbert transform:

$$z_x[n]=x[n]+j\tilde{x}[n]=a_x[n]e^{j\varphi_x[n]} \quad (1)$$

$$z_{y_i}[n]=y_i[n]+j\tilde{y}_i[n]=a_{y_i}[n]e^{j\varphi_{y_i}[n]} \quad (2)$$

where $a_x[n]$ and $a_{y_i}[n]$ are instantaneous amplitudes and the symbol tilde denotes the Hilbert transform. The fMRI time series are assumed to satisfy Bedrosian's requirement, namely that instantaneous amplitudes in Eqs. (1) and (2) are slow-varying signals and exponential terms are narrow-band signals having non-overlapping spectra with instantaneous amplitudes [Omidvarnia et al., 2016]. The DRePS measure associated with the voxel $x[n]$ is then computed as:

$$\psi_x[n]=\frac{1}{M-1}\sqrt{\left\{\sum_{i=1}^{M-1} cos\left(\varphi_x[n]-\varphi_{y_i}[n]\right)\right\}^2+\left\{\sum_{i=1}^{M-1} sin\left(\varphi_x[n]-\varphi_{y_i}[n]\right)\right\}^2}. \quad (3)$$

The function $\psi_x[n]$ quantifies the instantaneous mean phase coherence between $x[n]$, at the center of the moving cube and its 26 adjacent voxels (i.e., all faces, edges and corners of the central voxel). A grey matter DRePS time series map (which is 4 dimensional, having three spatial dimensions and time at the same resolution as the original fMRI time series) is constructed within the frequency band of interest (here, 0.03–0.07 Hz) by calculating $\psi_x[n]$ at every grey matter voxel [Omidvarnia et al., 2016]. The DRePS time series of each voxel represents its simultaneous phase relationship with its nearest neighbours. The applicability and usefulness of narrow-band (0.03–0.07 Hz) filtering in fMRI phase synchrony analysis has been already outlined in previous studies [Glerean et al., 2012; Ponce-Alvarez et al., 2015]. We previously evaluated this requirement and its consequences for DRePS analysis in [Omidvarnia et al., 2016] and showed that an expansion of the narrow-band filter of 0.03–0.07 Hz to a wider filter of 0.01–0.09 Hz in dynamic local fMRI connectivity analysis may affect the results. Whilst beyond the scope of the present study, this issue warrants further investigation.

Step B: Downsampled Band Amplitude Fluctuation

Combining the information of millisecond fluctuations in IEDs and much slower haemodynamic responses (several seconds) is challenging. To reduce the temporal resolution of the target EEG channel, we calculated its power envelope (i.e., BAF) using the Hilbert transform. The analysis of BAF within specified frequency bands gives an indirect way to assess event-level activities in scalp EEG signals [Hipp et al., 2012]. BAF signal denotes the power envelope of a filtered EEG signal $X[n,\Delta f]$, calculated from its analytic associate using the Hilbert transform:

$$BAF[n,\Delta f]=|X[n,\Delta f]+j\tilde{X}[n,\Delta f]|=\sqrt{X^2[n,\Delta f]+\tilde{X}^2[n,\Delta f]} \quad (4)$$

where $\tilde{X}[n,\Delta f]$ is the Hilbert transform of $X[n,\Delta f]$, $\Delta f=[f_2-f_1]$ is the band-pass frequency interval of the BAF, $|.|$ denotes the absolute value operator and $j=\sqrt{-1}$. A data reduction step was applied in order to bring $BAF[n,\Delta f]$ to the temporal resolution of fMRI. This was done by downsampling the BAF envelope to the T_R resolution, leading to a downsampled-BAF (DS-BAF) signal associated with the target EEG electrode for each patient. To ensure that this downsampling step does not ruin critical information, we inspected the frequency content of all subject-specific BAF signals using Morlet wavelet transform (see Fig. 3 as an example for Patient 1). For all patients, most BAF time-frequency information was below the fMRI Nyquist frequency (here, $1/2T_R=0.167$ Hz) which allowed the downsampling step on BAFs without significant loss.

The choice of the frequency band Δf in Eq. (4) is crucial for obtaining meaningful BAF signals from EEG recordings. In this study, we did not follow the traditional view of EEG filtering into the common frequency bands ($\delta, \theta, \alpha, \beta, \gamma$), as the spectral content of IEDs may overlap with multiple EEG bands. Instead, we obtained the optimal frequency interval $\Delta f=[f_1\ f_2]$ ($f_1<f_2$, see Eq. (4)) of a target EEG channel by maximizing the similarity between its associated DS-BAF and binary IED markup by a neurologist (DNV). The cut-off frequencies f_1 and f_2 were varied over the ranges $1\le f_1\le 19$ Hz and $2\le f_2\le 20$ Hz in steps of 1 Hz. For each frequency pair of (f_1, f_2), the resulting DS-BAF was treated as the output of a binary classifier with the IED markup as its true class labels through a multiple thresholding procedure (MATLAB command *perfcurve*). Performance of each classifier was quantified by the area under its associated receiver operating characteristic (ROC) curve (so called AUC). The frequency pair with maximum AUC was chosen as the optimal Δf for BAF extraction.

Step C: Analysis of DRePS-BAF Coupling Using Morlet Wavelet Coherence

Due to the time-varying dynamics of fMRI brain connectivity [Chang and Glover, 2010; Liu and Duyn, 2013; Ponce-Alvarez et al., 2015; Zalesky et al., 2014] as well as time-varying behaviour of scalp EEG [Omidvarnia et al., 2014], we employed a time-frequency approach to quantify the temporal coupling between EEG and fMRI connectivity over the scanning session. Wavelet transform coherence (WTC) analysis [Grinsted et al., 2004] based on the Morlet wavelet transform was used to investigate scale-dependent similarities between DRePS and DS-BAF. The Morlet type of mother wavelet is a Gaussian-windowed complex sinusoid with good time-frequency localization [Torrence and Compo, 1998]. It has been shown to be a useful computational tool for studying dynamic interactions between neuronal oscillators and the mechanisms underlying epilepsy [Li et al., 2007]. The Morlet wavelet transform function $W_x[n,s]$ is obtained by successive convolution of the time-shifted and scaled versions of the Morlet mother wavelet $\psi_0[n]$ with the input signal $x[n]$ [Grinsted et al., 2004]:

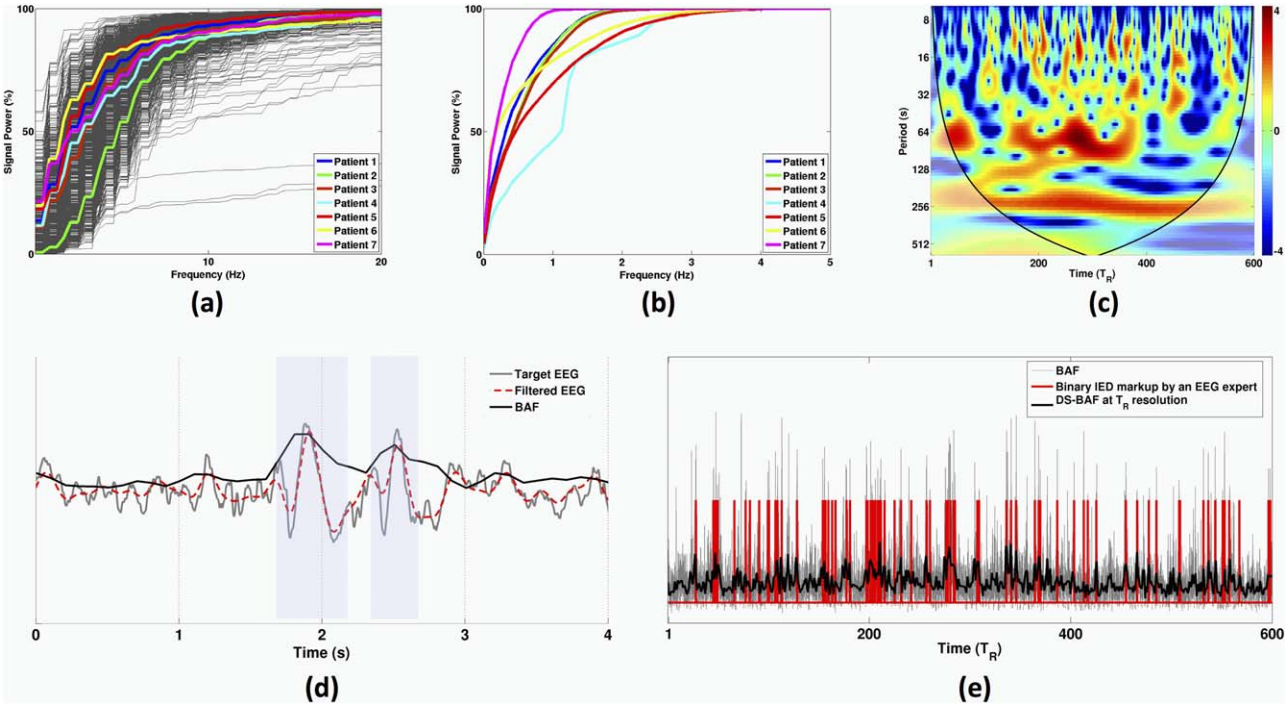

Figure 3.

(a) Subject-specific cumulative average band power of one-second segmented IEDs for all patients (500 ms before to 500 ms after each IED onset). The bold curves represent mean signal powers over all IED segments. (b) Subject-specific cumulative signal power of the BAF envelopes associated with target EEG channels listed in Table I. (c) Morlet wavelet transform of an exemplary DS-BAF over the entire scanning session (i.e., 1800 s equal to 600 T_R's). The bold curves on the sides of the time-frequency plane represent the cone of influence (see Step C: Analysis of DRePS-BAF coupling using Morlet wavelet coherence section). (d) Example of a target EEG signal including two marked IED events, its band-pass filtered version and its associated BAF. The blue shaded boxes show the marked IEDs. (e) Correspondence between a BAF envelope, its downsampled version (DS-BAF) and IED markup by the neurologist. [Color figure can be viewed at wileyonlinelibrary.com]

$$W_x[n,s]=\sqrt{\delta t/s}\sum_{n'=1}^{N}x[n']\psi_0^*\{[n-n'](\delta t/s)\}, \tag{5}$$

where δt is the sampling time step, s is the wavelet scale, the asterisk $*$ denotes the complex conjugate and the mother wavelet ψ_0 is defined as:

$$\psi_0[n]=\pi^{-1/4}e^{j\omega_0 n}e^{-n^2/2}, \tag{6}$$

where ω_0 is the controlling parameter of time-scale resolution. The $W_x[n,s]$ quantifies signal power of $x[n]$ at time n and the pseudo-frequency proportional to $1/s$. Throughout this paper, we have used the terms 'frequency' and 'scale', interchangeably, considering their direct (inverse) relationship. Due to the complex nature of $\psi_0[n]$, instantaneous phase information of $x[n]$ is also encoded into the transform. At very wide scales (i.e., very low frequencies), the length of the scaled wavelet approaches the entire length of the input signal leading to considerably poor temporal localization and significant edge-effects in the time-frequency plane. A 'cone of influence' is, therefore, introduced in the wavelet domain to exclude unreliable Morlet wavelet transform values under such circumstances.

The amount of joint Morlet wavelet transform power between two signals $x[n]$ and $y[n]$ can be quantified using the WTC magnitude function $R^2[n,s]$:

$$R^2[n,s]=\frac{|\mathrm{Smooth}\{s^{-1}W_{xy}[n,s]\}|^2}{|\mathrm{Smooth}\{s^{-1}W_x[n,s]\}|^2\ \times\ |\mathrm{Smooth}\{s^{-1}W_y[n,s]\}|^2}, \tag{7}$$

where Smooth{.} is a two dimensional spectro-temporal smoothing filter (here, a Gaussian function) and $W_{xy}[n,s]$ is the cross-wavelet transform between $x[n]$ and $y[n]$ defined as:

$$W_{xy}[n,s]=\ W_x[n,s]\ \times\ W_y^*[n,s]. \tag{8}$$

Following previous studies [Chang and Glover, 2010; Grinsted et al., 2004], we chose the value of $\omega_0=6$ for $\psi_0[n]$ as an acceptable resolution trade-off in the time-scale plane. $R^2[n,s]$ always takes values between 0 and 1 with

higher quantities implying stronger localized coherence in the time-frequency domain. In this study, wavelet coherence analysis of each patient resulted in a five dimensional WTC map in which each voxel was associated with a time-scale representation of DRePS-BAF coupling. The wavelet coherence analysis was carried out using a publicly released MATLAB toolbox available at http://www.glaciology.net/wavelet-coherence.

Steps D–E: Time-Frequency Thresholding and T-F Patch Ratio Analysis

To identify regions where there was strong coupling between DRePS and DS-BAF, we calculated the 'T-F patch size ratio' at each voxel. Beginning with the wavelet coherence plane for each voxel (Fig. 2a), only values outside the cone of influence of wavelet edge effects[2] and between frequencies 0.002–0.04 Hz [Omidvarnia et al., 2016] were considered (Fig. 2b). These values were thresholded at the 95th percentile to obtain 'T-F patches' (Fig. 2c). The ratio was calculated as the sum of values within patches divided by the sum of all values outside the cone of influence. This voxel-wise analysis yielded a 3D DRePS-BAF coupling map for each patient which was thresholded at the 99th percentile of its voxel population.

GLM-Based Standard EEG-fMRI Analysis

In addition to the proposed DRePS-BAF coupling framework, we also analysed the data with the commonly used EEG-fMRI analysis based on a GLM [Baudewig et al., 2001] and using the SPM8 toolbox. This was done to elucidate whether the DRePS-BAF coupling method provides different information to standard EEG-fMRI analysis. Three regressors related to manually determined IED onsets were included after convolving with the canonical hemodynamic response function (HRF) as well as its time and dispersion derivatives. Also, nuisance signals (six motion parameters as well as mean white matter and cerebrospinal fluid signals) were regressed out through the design matrix. Slow signal drifts with a period longer than 128 s were also removed (i.e., frequencies below ~0.008 Hz). A Student's *t*-test was then performed to determine the significance of the primary regressor of interest in the model. Statistical parametric maps were thresholded at a feature-defining uncorrected voxel height $P < 0.001$ and a Gaussian Random Field Theory cluster-level $P < 0.05$ to avoid a potentially inflated false positive rate [Eklund et al., 2016].

[2]The term 'cone of influence' was defined by [Grinsted et al., 2004]. The influence of wavelet edge effects becomes more pronounced the larger the period of the wavelet relative to the length of the time-series data. Inside the cone of influence these effects are substantial, resulting in reduced confidence; specifically, this is the area in which the wavelet power caused by a discontinuity at the edge is at least e^{-2} of the value at the edge. In Figure 2b the cone of influence consists of the two black-masked 'half-cone-shaped' regions on the left and right of the unmasked portion of the DRePS-BAF wavelet coherence map.

RESULTS

BAF Analysis

We calculated the cumulative signal power of one-second IED segments (0.5 s before to 0.5 s after each IED onset) for all subjects. As Figure 3a shows, most IED power occurred below 20 Hz with 90% below 15 Hz (median; range 10–17 Hz). However, cumulative signal power of the continuous BAF extracted from the target EEG electrodes was much lower (below 3 Hz, see Fig. 3b). Whilst the spectral content of BAF may vary across patients and electrodes, it is always slower than its corresponding EEG signal (Fig. 3d). Figure 3e illustrates the downsampled BAF for one participant (Patient 1, with EEG pass-band of 3–5 Hz). It has a high similarity to the underlying binary IED markup, reflected in the associated maximum AUC value of 88.7%. Also, a significant amount of its frequency content is below the T_R time-period (see high-value red patches in Fig. 3c as an example). See Figure 4 and Table II for the ROC analysis results of all patients.

The maximum AUC values over patients varied from 73.6% (Patient 3) to 88.7% (Patient 1). The associated optimal frequency bands were specific to everyone, with high-pass cut-off $\mathbf{f_1}$ ranging between 1 and 5 Hz, and low-pass cut-off $\mathbf{f_2}$ ranging between 5 and 7 Hz. These values are likely to reflect individual variability in the frequencies and patterns of IEDs. In some cases, there were several frequency bands with comparable AUC values (e.g., elements with hot colour coding in the performance matrices of Fig. 4). Therefore, the proposed ROC analysis scheme here may not be a one-to-one mapping between DS-BAFs and optimal frequency intervals.

DRePS-BAF Coupling and Standard EEG-fMRI Maps

Patient 1

This 43-year-old man had tuberous sclerosis with focal dyscognitive seizures starting from age 10. Visual inspection of his anatomical MRI showed multiple tubers in the left temporal lobe, two large tubers in the left parietal area and left anterior cingulate, in addition to left hippocampal sclerosis. Interictal epileptiform discharges were most commonly seen on the left with fewer discharges on the right. The left fronto-temporal region was the source of his most active interictal epileptiform abnormality, and corresponded to the region of hypo-metabolism on FDG-PET imaging as well as hyper-perfusion on ictal-interictal SPECT.

Mean IED waveforms of this patient showed activity broadly over left temporal and frontal electrodes, and was

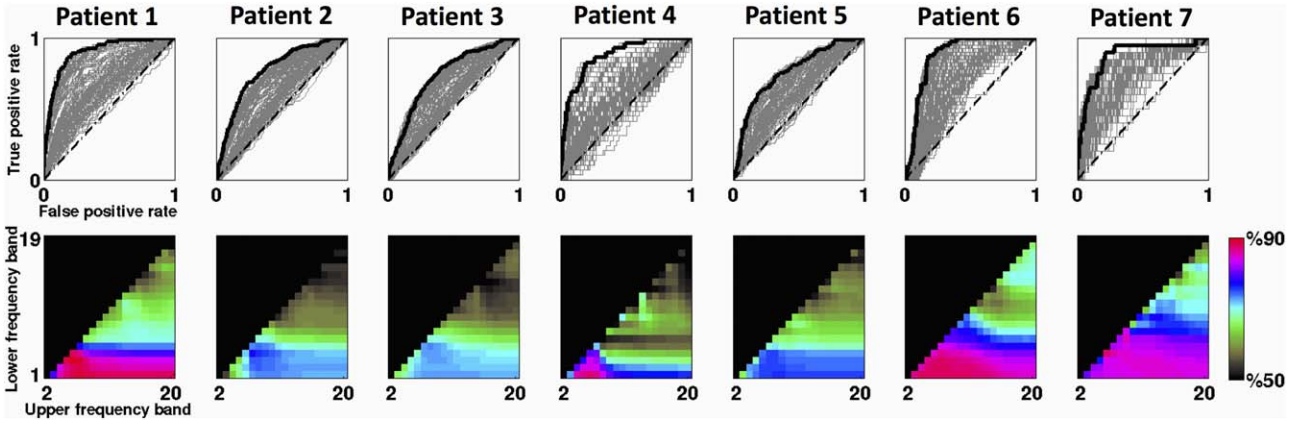

Figure 4.

Selection of optimal EEG filtering band for BAF analysis of each participant. The first row represents the ROC curves of all possible frequency bands for each patient. The ROC curve that yielded the maximum AUC value has been highlighted in bold. The second row demonstrates the AUC values (in %) associated with all possible frequency bands with 1-Hz steps spanning the range of 1–20 Hz. AUC values below 50% have been blacked out. Warmer colours denote superior performance; in some cases, optimum AUC values were quite similar in several frequency bands. [Color figure can be viewed at wileyonlinelibrary.com]

maximal at T7 which we chose as the target electrode (Fig. 5a,b). The DRePS-BAF coupling map for this patient (Fig. 5c) showed multiple suprathreshold brain areas including the ipsilateral insular cortex and mesial temporal lobe (proximate to the suspected seizure onset zone), contralateral cerebellum, posterior cingulate cortex and primary visual cortex. Standard EEG-fMRI map showed increased BOLD activity in anterior fronto-tempor-insular cortices and decreased activity at posterior cingulate cortex (Fig. 5d).

Patient 2

This 42-year-old female started having seizures at age 7. Structural MRI showed periventricular nodular heterotopia with a predominantly intra-sylvian distribution. There was also a relatively large lesion and diffuse cortical abnormalities in the left temporal lobe. No visible change of metabolism or perfusion was observed in her PET or SPECT data. Focal epileptiform discharges were observed across the left temporal region with largest mean IED amplitude at T7 (Fig. 6a,b). The DRePS-BAF coupling map (Fig. 6c) demonstrated high wavelet coherence over ipsilateral temporal neo-cortex, ipsilateral insula, bilateral periventricular areas and precuneus. Standard EEG-fMRI *T*-map showed decreased BOLD activity in bilateral temporal cortices, cingulate cortex as well as contralateral cerebellum and increased BOLD activity across contralateral periventricular regions (Fig. 6d).

TABLE II. Summary of the maximum AUC values and their associated frequency intervals obtained from ROC analysis of all patients

Patient	Maximum AUC (%)	Corresponding frequency band (Hz)
1	88.7	3–5
2	77.0	4–6
3	73.6	5–7
4	87.3	1–5
5	75.8	1–7
6	87.9	1–6
7	87.1	4–5

Patient 3

Patient 3 was a 29-year-old female with temporal lobe epilepsy and seizure onset at the age of 16. She had no visible brain abnormality on structural MRI. The left anterior temporal lobe was associated with hypo-metabolism and ictal hyper-perfusion observed on PET and SPECT, respectively. Mean IED waveform showed epileptiform activity over temporal lobe EEG electrodes, with highest amplitude at T7 (Fig. 7a,b). The DRePS-BAF coupling map showed suprathreshold areas at the ipsilateral insula (proximate to the suspected seizure onset zone), bilateral parietal cortex and cerebellum (Fig. 7c). No significant voxels were detected in the standard GLM analysis. Trending *T*-values (>2.3) were observed in the GLM map near the suspected seizure onset zone, but no voxel survived cluster correction.

Patient 4

This 40-year-old female with a clinical diagnosis of frontal lobe epilepsy had seizures beginning at 3 months of age. Subtle structural abnormalities were noted in the right frontal lobe but whether these are epileptogenic remains debated. A small linear track of T2 hyperintensity is also

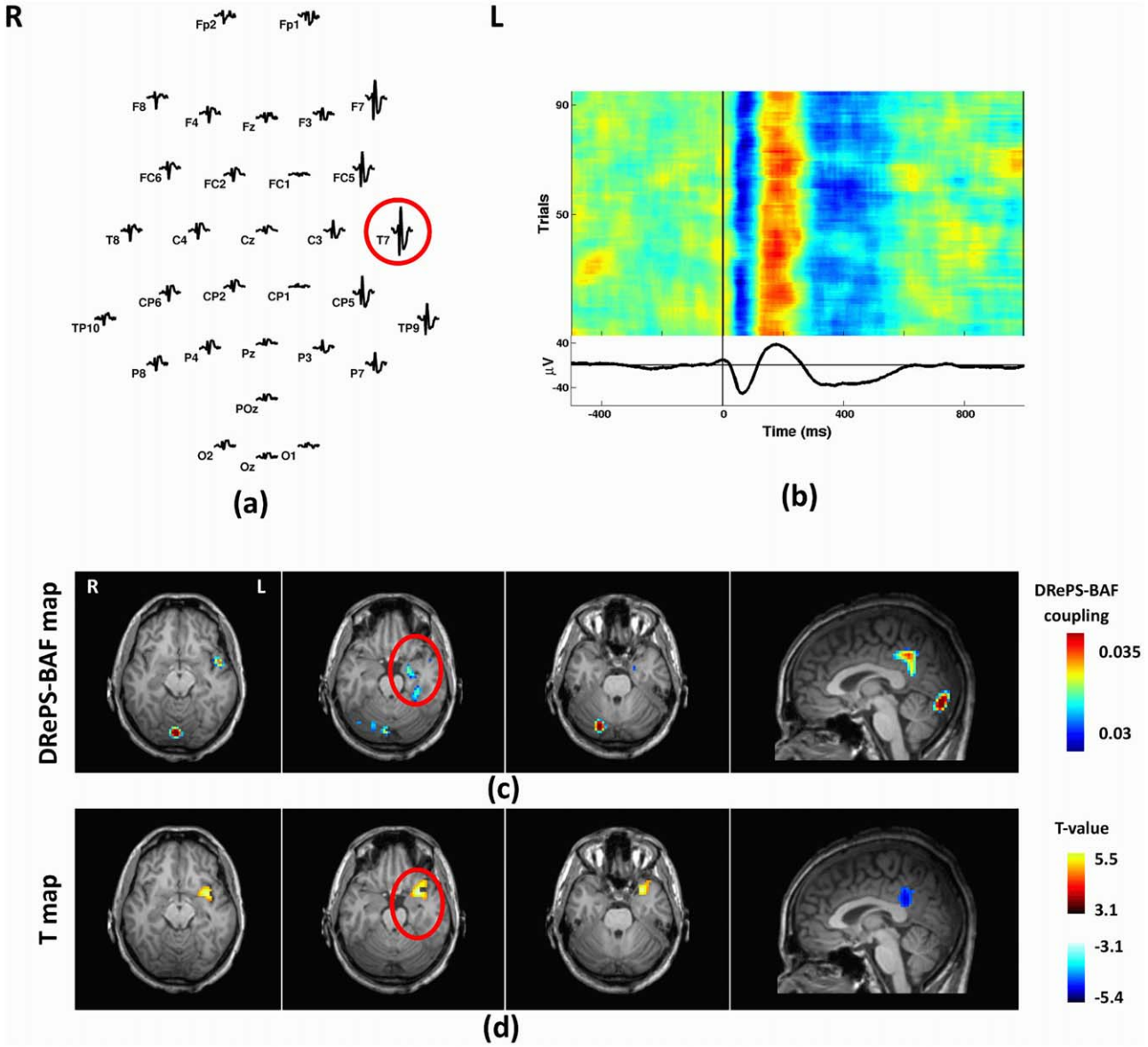

Figure 5.

Analysis results of Patient 1: (a) Spatial distribution of the mean spikes over all EEG electrodes, (b) Average IED waveform at T7 as the target electrode, (c) DRePS-BAF coupling map, (d) Standard EEG-fMRI *T*-map. All functional brain maps are overlaid onto the patient's own anatomical T_1 images. The suspected seizure onset zone as determined by standard clinical investigation (see Table I) has been highlighted by red circles on the brain maps. In this patient, both methods reveal suprathreshold clusters within the region of the presumed seizure focus (anterior fronto-tempor-insular cortices) although the clusters of each method are adjacent rather than overlapping. Both methods also show high values in the posterior cingulate cortex. [Color figure can be viewed at wileyonlinelibrary.com]

present at the right superior temporal gyrus related to previous depth electrode implantation. FDG-PET and SPECT showed hypo-metabolism and ictal hyper-perfusion of the right frontal and temporal lobes, respectively. The largest IED amplitudes were seen across frontal and temporal areas, and were maximal at electrode Fz. DRePS-BAF coupling showed spatial clusters of voxels within the suspected seizure onset zone as well as precuneus and contralateral cerebellum (Fig. 8c). Standard EEG-fMRI showed increased BOLD activity in the ipsilateral temporo-parietal lobe and the supplementary motor area (Fig. 8d). We observed fMRI voxels with *T*-values up to 1.5 in the right

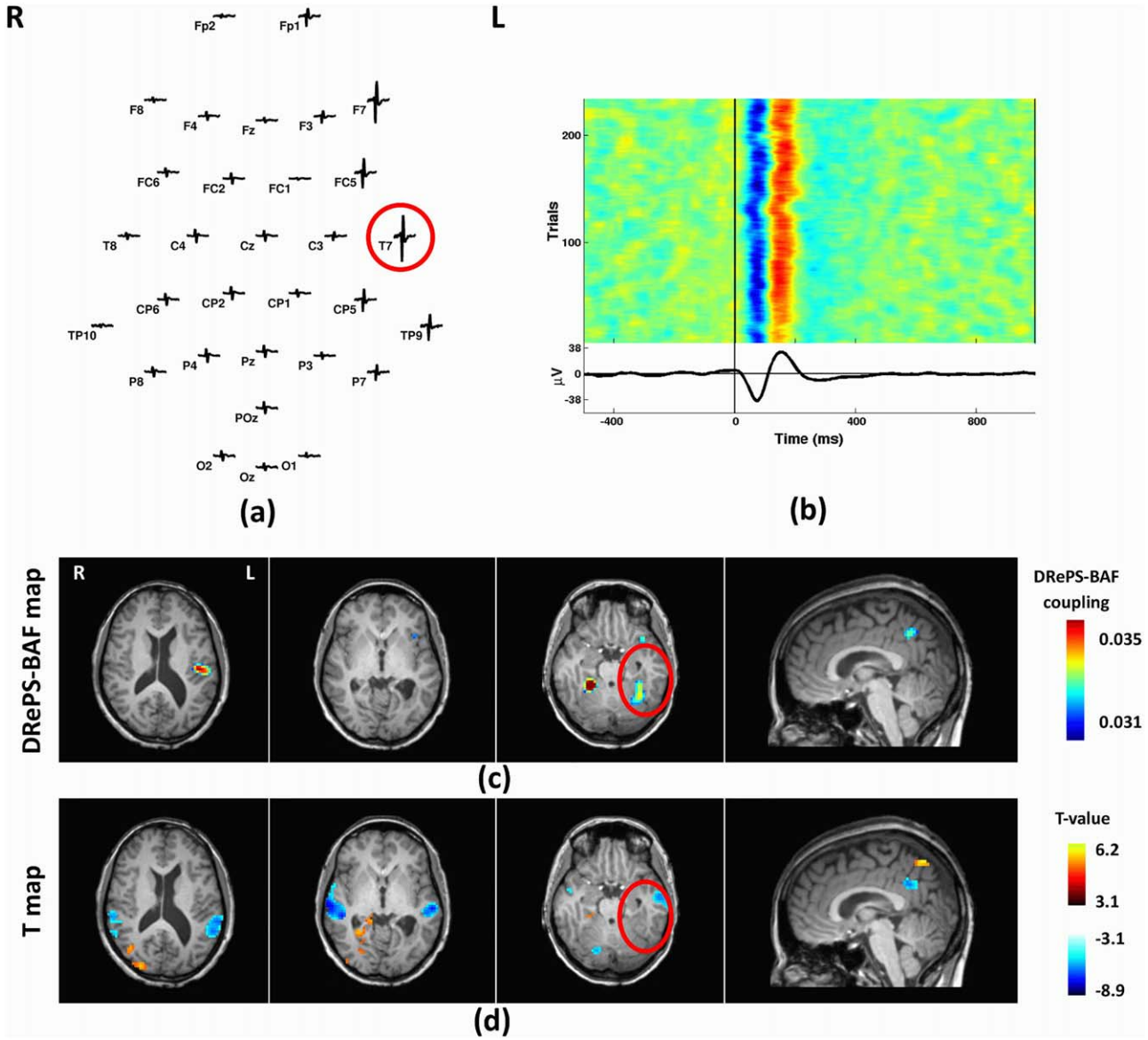

Figure 6.

Analysis results of Patient 2: (a) Spatial distribution of the mean spikes over all EEG electrodes, (b) Average IED waveform at T7 as the target electrode, (c) DRePS-BAF coupling map, (d) Standard EEG-fMRI *T*-map. All functional brain maps are overlaid onto the patient's own anatomical T_1 images. The suspected seizure onset zone as determined by standard clinical investigation (see Table I) has been highlighted by red circles on the brain maps. In this patient, both methods show spatial clusters within the suspected epileptic zone. Also, there are adjacent clusters with both methods at posterior cingulate cortex and ipsilateral temporal cortex. [Color figure can be viewed at wileyonlinelibrary.com]

frontal lobe (near the suspected epileptic region), but these voxels did not survive cluster correction.

Patient 5

This 41-year-old male with seizure onset at 16 was previously diagnosed with right temporal lobe epilepsy, and treated with a right anterior temporal lobectomy, however, his temporal seizures continued to occur. PET demonstrated hypo-metabolism on the right and hyper-metabolism across the left temporal areas. Also, SPECT showed ictal hyper-perfusion of the right fronto-insular cortex and right posterior temporal areas. However, mean IED waveforms showed comparable epileptiform activity

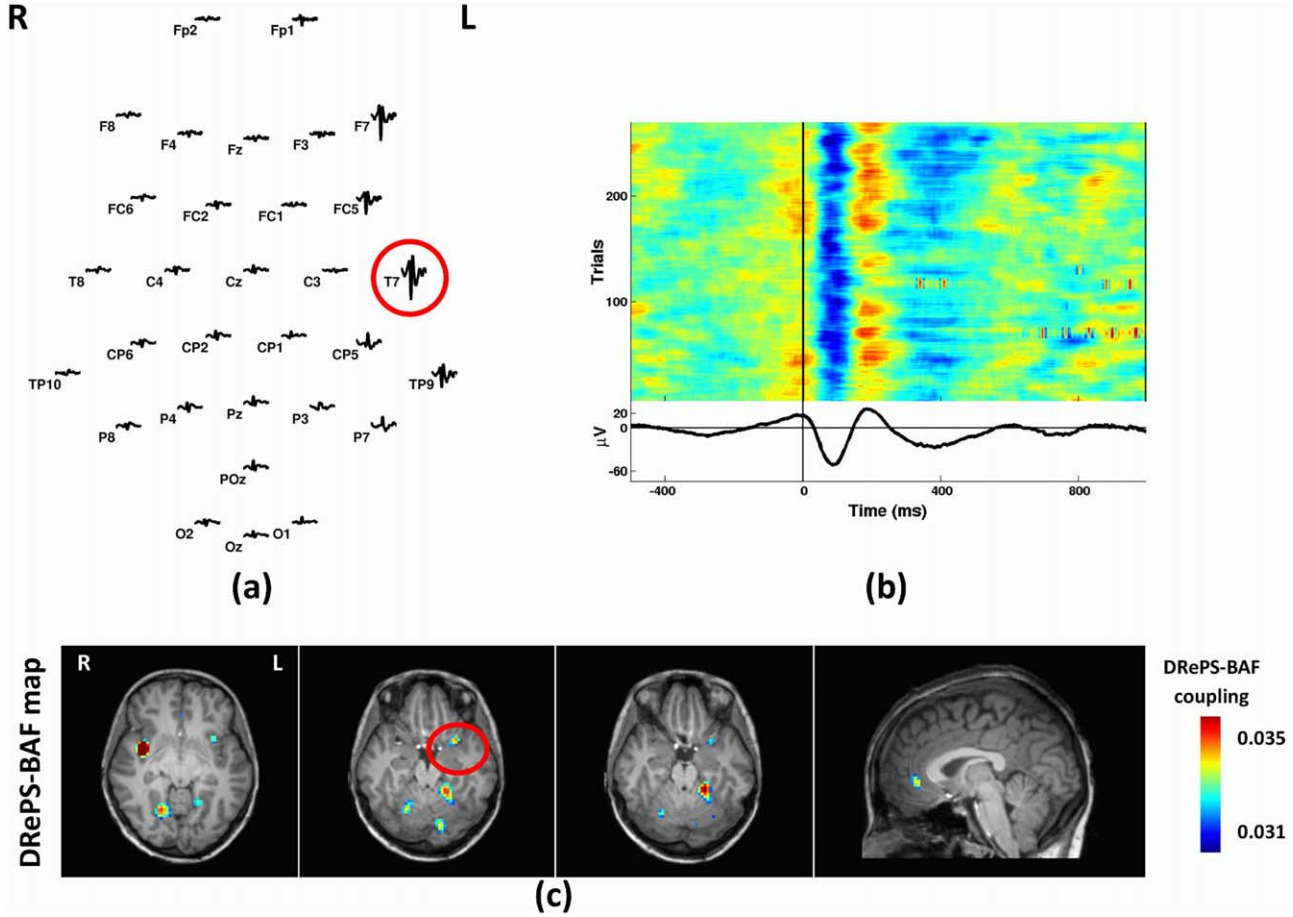

Figure 7.

Analysis results of Patient 3: (a) Spatial distribution of the mean spikes over all EEG electrodes, (b) Average IED waveform at T7 as the target electrode, (c) DRePS-BAF coupling map. All functional brain maps are overlaid onto the patient's own anatomical T_1 images. The suspected seizure onset zone as determined by standard clinical investigation (see Table I) has been highlighted by red circles on the axial map. The DRePS-BAF map shows a spatial cluster within the suspected epileptic zone. There were no statistically significant voxels in the GLM map. [Color figure can be viewed at wileyonlinelibrary.com]

in both temporal lobes, with a maximal amplitude in the left hemisphere at T7 (Fig. 9a,b). We classified this patient as bilateral TLE. The DRePS-BAF coupling map showed suprathreshold clusters in the right temporal neo-cortex, bilateral parietal lobule, precuneus, and the left anterior temporal lobe. On the contrary, GLM map emphasized the left hemisphere including inferior parietal and temporal lobes (Fig. 9d). Both maps overlapped over the left inferior parietal lobe and posterior cingulate cortex.

Patient 6

Patient 6 was a 26-year-old male with seizure onset at age 13 years, with a clinical diagnosis of right frontal lobe epilepsy. Structural MRI was normal. PET showed hypo-metabolism of left frontal areas. Ictal SPECT suggested hyper-perfusion to the right temporal, mesial frontal and right frontal polar cortices. Mean IED waveforms showed maximal amplitude at Fp2 (Fig. 10a,b). The most notable areas in the DRePS-BAF coupling map (Fig. 10c) included the ipsilateral cerebellum and precuneus. Trending wavelet coherence values were seen in ipsilateral frontal cortex (near the suspected seizure onset zone), but these voxels did not survive thresholding. The frontal lobes were dominant in the standard EEG-fMRI analysis with significantly increased BOLD activity. Decreased BOLD activity was observed in the contralateral visual cortex (Fig. 10d).

Patient 7

This patient was a 28-year-old female with a clinical diagnosis of temporal lobe epilepsy, and seizure onset at age 8 years. Structural MRI did not show any epileptogenic abnormality. PET showed hypo-metabolism in the right posterior temporal

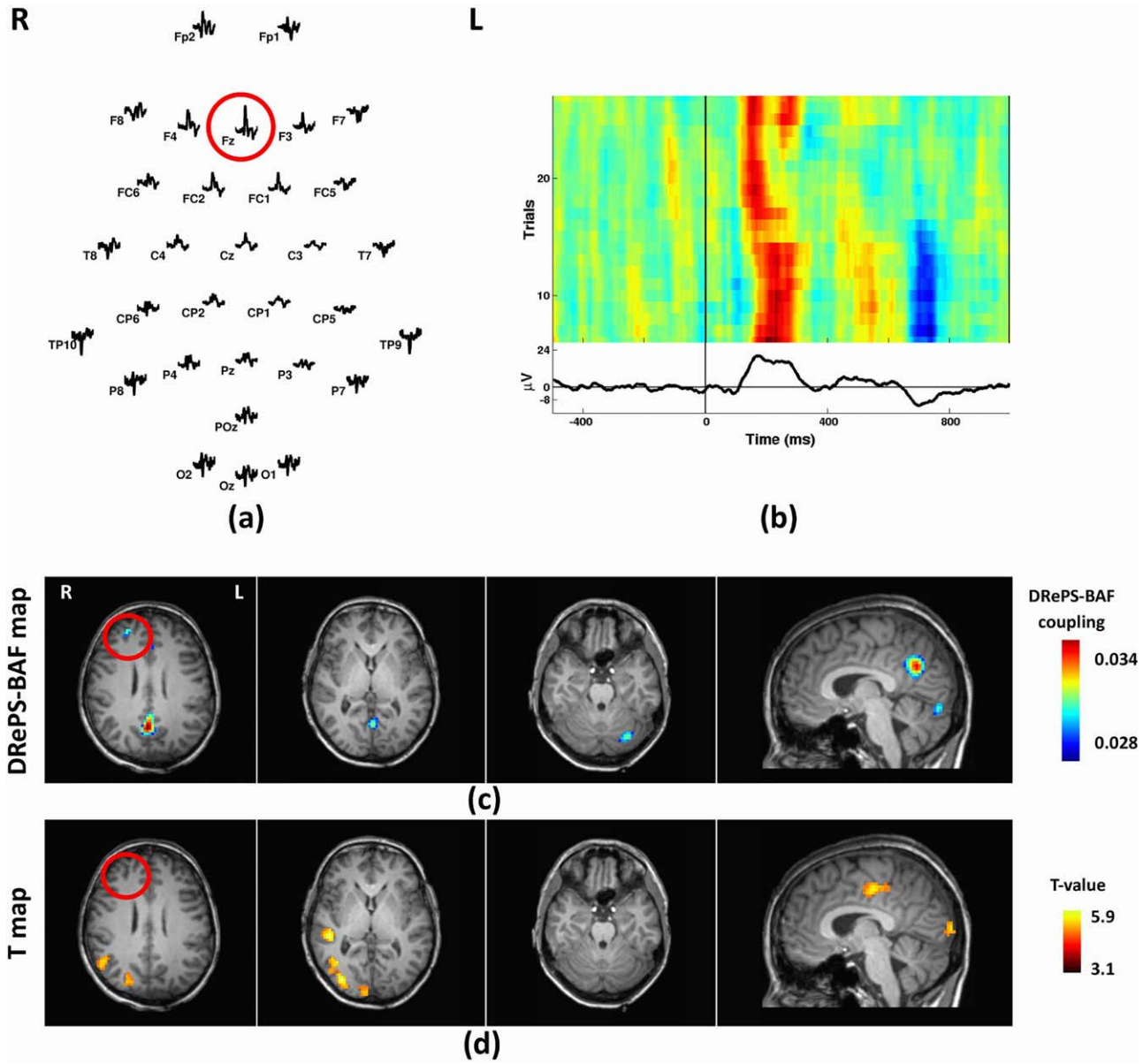

Figure 8.

Analysis results of Patient 4: (a) Spatial distribution of the mean spikes over all EEG electrodes, (b) Average IED waveform at Fz as the target electrode, (c) DRePS-BAF coupling map, (d) Standard EEG-fMRI *T*-map. All functional brain maps are overlaid onto the patient's own anatomical T_1 images. The suspected seizure onset zone as determined by standard clinical investigation (see Table I) has been highlighted by red circles on the brain maps. In this patient, The DRePS-BAF map shows a cluster within the suspected epileptic zone, whereas the GLM map did not exhibit significant voxels in this region. [Color figure can be viewed at wileyonlinelibrary.com]

cortex, and ictal SPECT showed hypo-perfusion at the same area. Mean IED waveforms indicated T8 as the most dominant IED channel (Fig. 11a,b). The DRePS-BAF coupling map showed suprathreshold voxels proximate to the previous surgery in addition to precuneus and contralateral visual cortex (Fig. 11c). The GLM *T*-map (Fig. 11d) demonstrated widespread decreased BOLD activity across bilateral occipital and frontal cortices. We observed trending *T*-values (>2.3) near the suspected epileptic region, but these voxels did not survive cluster correction.

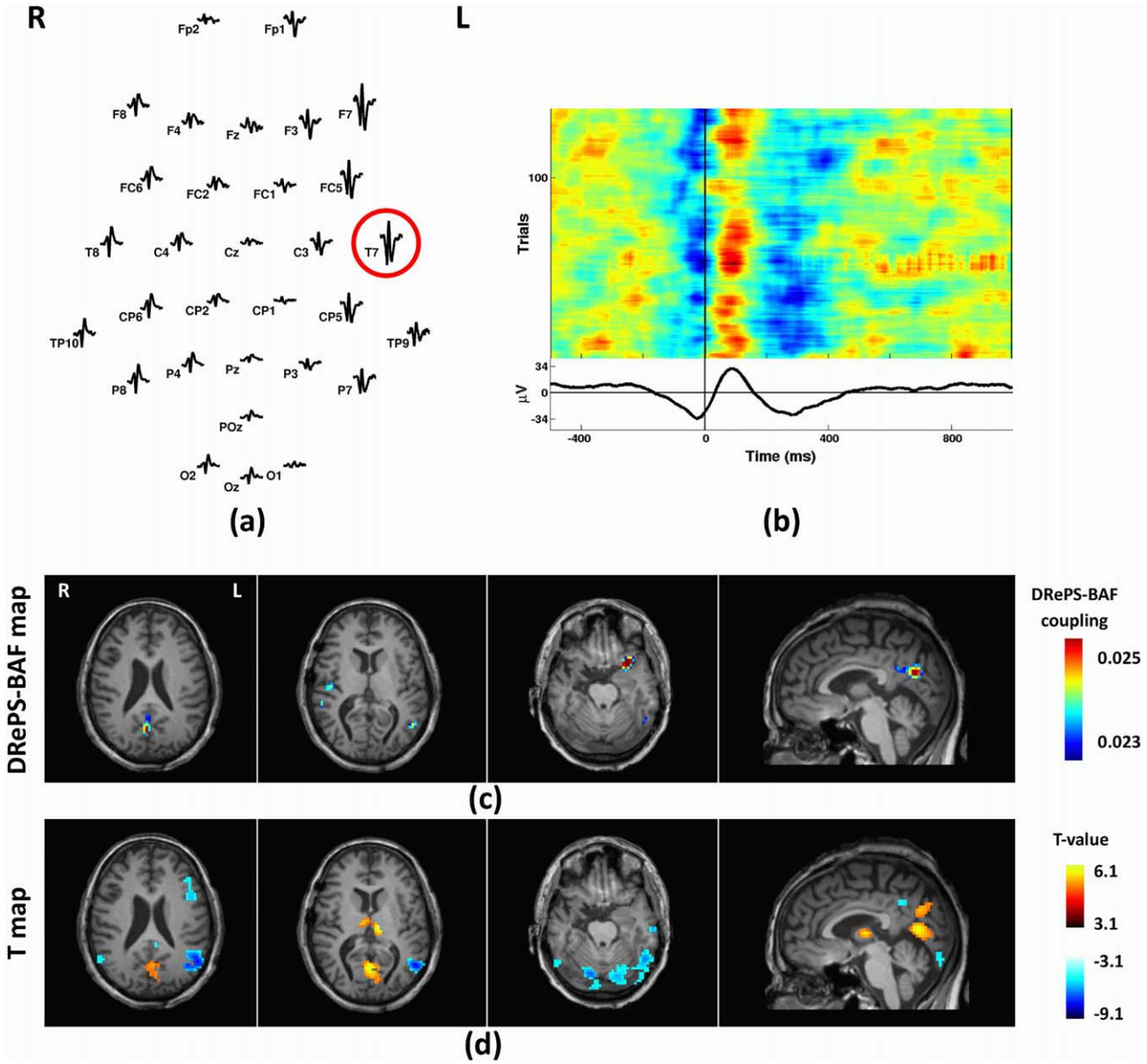

Figure 9.

Analysis results of Patient 5: (a) Spatial distribution of the mean spikes over all EEG electrodes, (b) Average IED waveform at T7 as the target electrode, (c) DRePS-BAF coupling map, (d) Standard EEG-fMRI *T*-map. All functional brain maps are overlaid onto the patient's own anatomical T_1 images. This patient has uncertain bilateral foci, as determined by standard clinical investigation (see Table I) so the onset zone cannot be highlighted. The two maps show overlapping clusters over the left inferior parietal lobe and posterior cingulate cortex. The DRePS-BAF map exhibits a particularly high-value cluster in the left anterior temporal lobe (contralateral to the previous surgery). [Color figure can be viewed at wileyonlinelibrary.com]

DISCUSSION

Establishing DRePS-BAF Coupling as an EEG-fMRI Data Fusion Framework

Simultaneous EEG-fMRI data fusion techniques are increasingly used in clinical assessment of epilepsy, as the millisecond temporal resolution of EEG recordings and millimetre spatial resolution of the fMRI provide higher accuracy in both domains than would be possible with just one of these modalities [Mulert and Lemieux, 2010; Salek-Haddadi et al., 2003]. However, tracking the coupling between hemodynamic changes and their underlying

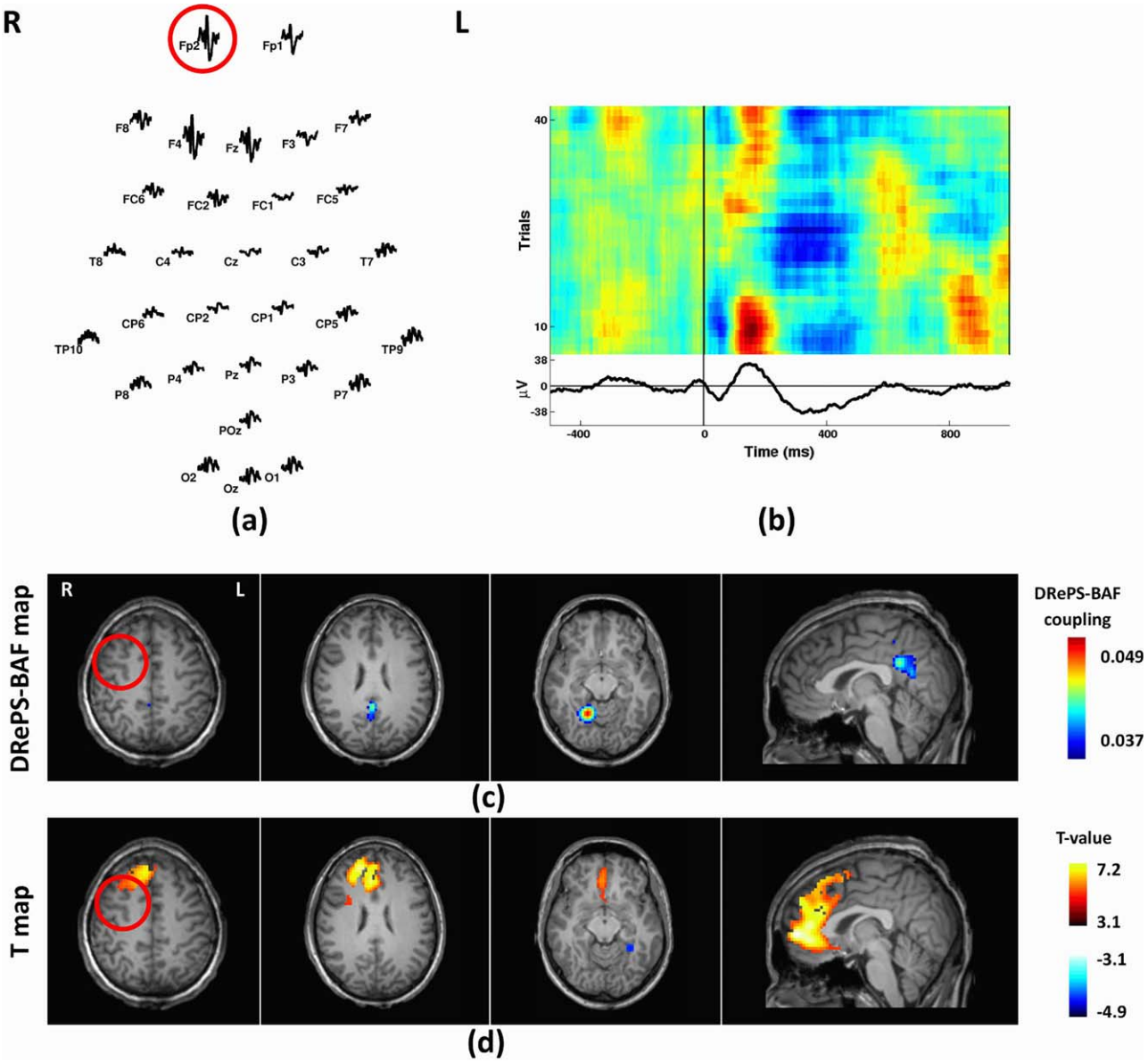

Figure 10.

Analysis results of Patient 6: (a) Spatial distribution of the mean spikes over all EEG electrodes, (b) Average IED waveform at Fp2 as the target electrode, (c) DRePS-BAF coupling map, (d) Standard EEG-fMRI *T*-map. All functional brain maps are overlaid onto the patient's own anatomical T_1 images. The suspected seizure onset zone as determined by standard clinical investigation (see Table I) has been highlighted by red circles on the brain maps. The GLM map shows significantly high *T*-values across ipsilateral frontal areas and also contralateral cerebellum (not depicted in the figure). The DRePS-BAF map exhibits high-value clusters in the ipsilateral cerebellum and precuneus. [Color figure can be viewed at wileyonlinelibrary.com]

electrophysiological activity is not a straightforward task in simultaneous EEG-fMRI. A particular difficulty in the case of epilepsy is that the onset of an IED will not necessarily be obvious on scalp EEG unless neuronal firing becomes temporally synchronous across a large cortical area [Tao et al., 2007]. Thus, if epileptiform activity evolves to synchronously occupy an increasingly large cortical area, then fMRI can potentially be sensitive to this evolution before it is detectable on EEG. It follows that there may not be a temporal coincidence between the start (or end) of IED events evident in the EEG recording and the corresponding hemodynamic response. Also, the fMRI response associated with IEDs does not necessarily conform to the 'canonical' HRF induced by an impulse event

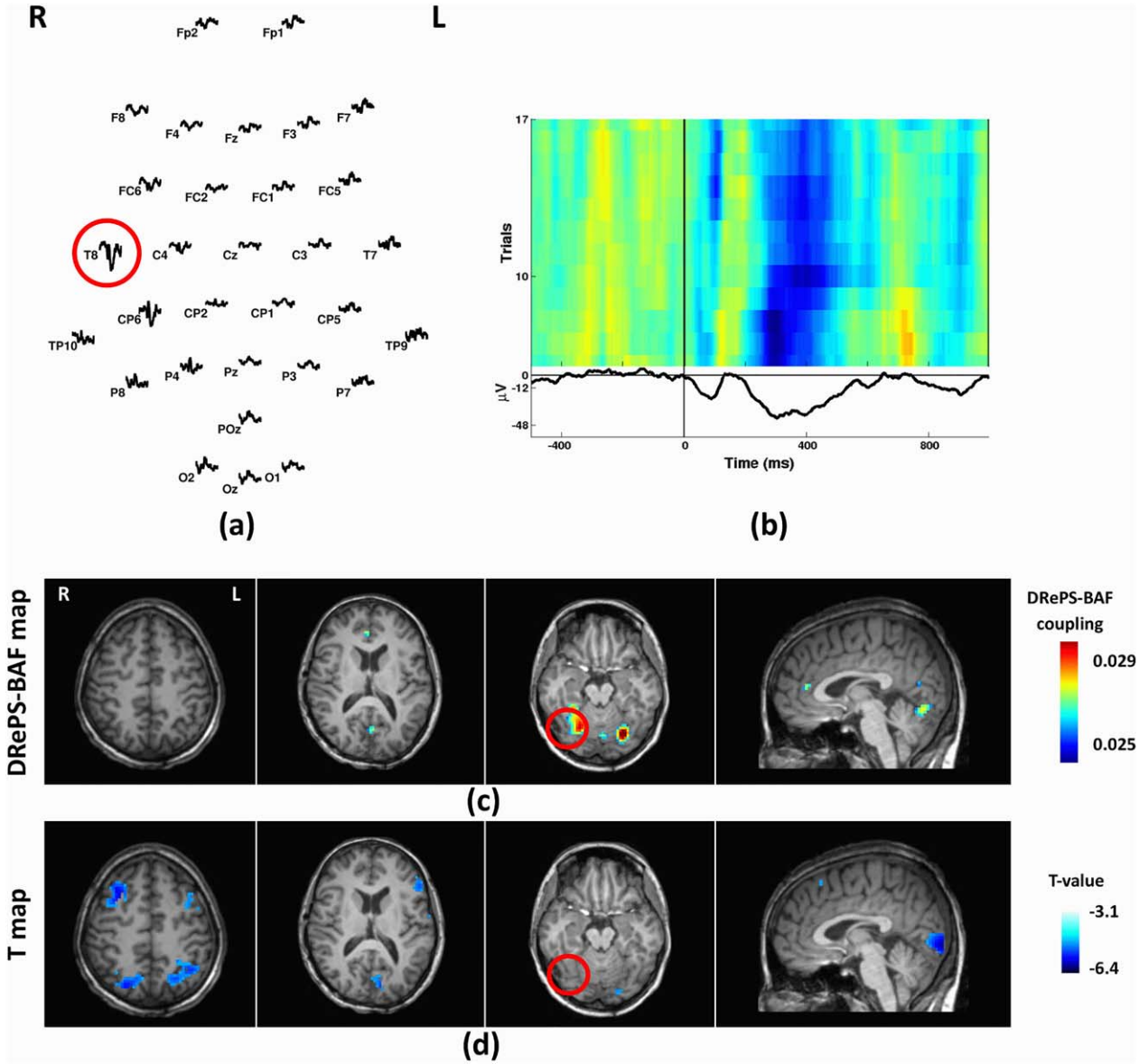

Figure 11.

Analysis results of Patient 7: (a) Spatial distribution of the mean spikes over all EEG electrodes, (b) Average IED waveform at T8 as the target electrode, (c) DRePS-BAF coupling map, (d) Standard EEG-fMRI *T*-map. All functional brain maps are overlaid onto the patient's own anatomical T_1 images. The suspected seizure onset zone as determined by standard clinical investigation (see Table I) has been highlighted by red circles on the brain maps. The DRePS-BAF map shows suprathreshold voxels superior and lateral to the previous surgery (suspected seizure focus). The GLM map shows wide-spread decreased BOLD activity across bilateral occipital and frontal cortices. Trending *T*-values (>2.3) are also observed near the suspected epileptic region, but these voxels do not survive cluster correction. [Color figure can be viewed at wileyonlinelibrary.com]

[Masterton et al., 2010, 2013; Salek-Haddadi et al., 2002]. Therefore, EEG-fMRI data fusion methods which reduce spike events to a binary timing mask with crisp on/off periods in relation to simultaneous BOLD changes may not capture a complete picture of brain areas involved in focal epilepsy. In contrast, our proposed analysis framework considers the continuous form of interictal EEG recordings accommodating more realistic presentation of the spikes. It offers a dynamic analysis approach for extraction of the time-varying coupling between fMRI local connectivity and interictal EEG in focal epilepsy. The framework takes advantage of Dynamic Regional Phase

Synchrony's (DRePS) ability to measure variable local functional connectivity at a temporal resolution of fMRI acquisition. This could be an improvement compared to time-averaged approaches that either assume temporal stationarity of fMRI connectivity, or attempt to account for temporal dynamics using sliding window approaches with much less temporal resolution than the original fMRI acquisition. Our framework yields patient-specific dynamic spatial maps of local connectivity coupling between fMRI and interictal EEG.

DRePS-BAF Coupling and its Time-Varying Nature

It is increasingly being recognised that epilepsy, including that arising from a focal origin, can affect wide-spread brain networks [Archer et al., 2014; Jackson et al., 2017; Warren et al., 2017]. This is likely to be a result of complex ictal and interictal network behaviours expressed as hyper-connectivity inside and outside the ictogenic zone. It is, therefore, important to find new ways of analysing wide-spread epileptogenic activity and interpreting its behaviour in relation to the dynamics of functional brain networks. Indeed we have recently shown that subsecond changes related to epileptic spikes may not only involve the epileptic foci, but also distributed brain network properties [Walz et al., 2017]. Dynamic brain connectivity is, therefore, a promising avenue for enhancing our understanding of focal epilepsy as a network disease.

It has been previously suggested that there is a proportional relationship between hemodynamic changes and the energy dissipation rate of their underlying brain regions [Kilner et al., 2005]. From this perspective, static ReHo analysis is a relevant metric for measuring the rate of brain metabolism [Aiello et al., 2015]. In our previous study we demonstrated that high DRePS power also occurs in high energy-demand areas of the healthy brain including the primary visual cortex and the default mode network [Omidvarnia et al., 2016]. It is also known that cerebral glucose metabolism and blood flow are directly related to interictal epileptiform spiking activity [Bittar et al., 1999] and these discharges will change the properties of simultaneously acquired EEG spectral power [Kilner et al., 2005]. This may explain the coupling between BAFs and DRePS time series observed in this study. However, to prove a relationship between DRePS and brain metabolism would require other measurements, such as simultaneous and dynamic FDG-PET (e.g., see [Villien et al., 2014]).

Limitations and Future Work

The primary aim of our study was to extract time-varying and direct links between interictal EEG at the scalp level, and concurrent regional connectivity changes in fMRI. Given the relatively small sample size of our focal epilepsy cohort, its clinical applicability needs to be verified by larger and more homogeneous groups in future studies. Nevertheless, the non-convergent results between DRePS-BAF and standard EEG-fMRI analyses we observed in individual subjects is interesting and likely to arise because DRePS-BAF considers the time-varying relationship of EEG and fMRI, whilst standard EEG-fMRI reduces the EEG signals to binary timings of the epileptiform events visible on the EEG.

BAF frequency band selection of the proposed approach needs the human IED markup at a target EEG electrode. This procedure is to some extent subjective and may not include low voltage events [van Graan et al., 2015]. Data driven detection of events, for example by incorporating information of multiple EEG channels simultaneously would allow for an unbiased multichannel framework. To this end, multivariate EEG features such as generalized phase synchrony [Omidvarnia et al., 2013], entropy measures or multivariate mutual information [Batina et al., 2010] may be considered instead of the single-channel BAF signal. In this case, incorporating time-varying global connectivity (e.g., see [Ponce-Alvarez et al., 2015]) might be more relevant than the local view of DRePS. Also, dependence of the coupled DRePS-BAF brain regions to the choice of target electrode deserves more attention in future research. There is not necessarily a direct relationship between maximal spike amplitudes and their underlying cortical region due to the superposition of several EEG sources at the surface level. A more reliable approach would be to use intracranial EEG. Since we were limited to the scalp EEG recordings in this study, we relied on the location of the dominant IEDs across surface EEG electrodes in conjunction with visual inspection of structural MRI data for each patient. We also considered methods of source localization, but given insufficient number of electrodes in our EEG recordings, we felt it was more appropriate to simply report the scalp localization.

Dealing with the lags between scalp realization of neural activity and its associated hemodynamic response is an important concern in simultaneous EEG-fMRI analysis. The traditional solution to this problem is to convolve the IED timing's binary markup with the canonical HRF, and then investigate the relationship between the resulting signal and concurrent fMRI time series. However, this common practice assumes a linear time-invariant coupling between EEG and fMRI. In other words, the canonical HRF is considered as the impulse response function of a linear time-invariant system whose input is the IED markup and output is the fMRI time series. However, in the case of coupling between interictal EEG and regional changes of hemodynamic activity, there is considerable evidence that: (1) this relationship is not necessarily linear and time-invariant, and (2) the impulse response function derived from the IED timing's binary markup does not necessarily follow a canonical HRF [Masterton et al., 2010, 2013; Salek-Haddadi et al., 2002]. Therefore, we refrained

from convolving the DRePS and/or BAF signals with the standard HRF.

The results of this study suggest that there are differences between DRePS-BAF coupling maps and the corresponding standard EEG-fMRI maps. However, our interpretations are mainly based on the human expertise and biological plausibility of the maps. It is not possible to validate the observations in an objective way, unless there is a ground truth to serve as a benchmark. It may be possible via realistic simulations, where we know the ground truth. In future work, we also aim to develop appropriate null models to statistically test coupling between DRePS and BAF.

CONCLUSION

Dynamic coupling between brain local functional connectivity and the band power envelope of scalp EEG may reveal aspects of abnormal brain function not identified by either method alone. Our proof of principal study suggests the proposed method could be complementary to event-related EEG-fMRI analysis of focal epileptic discharges.

ACKNOWLEDGMENTS

We gratefully thank Mira Semmelroch, Donna Parker and Magdalena Kowalczyk for assistance with EEG-fMRI data acquisition and preprocessing. We also acknowledge the facilities, and the scientific and technical assistance of the National Imaging Facility (NIF) at the Florey node and The Victorian Biomedical Imaging Capability (VBIC).

REFERENCES

Abbott DF, Masterton RAJ, Archer JS, Fleming SW, Warren AEL, Jackson GD (2015): Constructing carbon fibre motion detection loops for simultaneous EEG-fMRI. Front. Neurol. 5:260.

Aiello M, Salvatore E, Cachia A, Pappatà S, Cavaliere C, Prinster A, Nicolai E, Salvatore M, Baron J-C, Quarantelli M (2015): Relationship between simultaneously acquired resting-state regional cerebral glucose metabolism and functional MRI: A PET/MR hybrid scanner study. NeuroImage 113:111–121.

Allen PJ, Polizzi G, Krakow K, Fish DR, Lemieux L (1998): Identification of EEG events in the MR scanner: The problem of pulse artifact and a method for its subtraction. NeuroImage 8: 229–239.

Allen PJ, Josephs O, Turner R (2000): A method for removing imaging artifact from continuous EEG recorded during functional MRI. NeuroImage 12:230–239.

Archer JS, Warren AEL, Stagnitti MR, Masterton RAJ, Abbott DF, Jackson GD (2014): Lennox-Gastaut syndrome and phenotype: Secondary network epilepsies. Epilepsia 55:1245–1254.

Attwell D, Laughlin SB (2001): An energy budget for signaling in the grey matter of the brain. J Cereb Blood Flow Metab 21: 1133–1145.

Batina L, Gierlichs B, Prouff E, Rivain M, Standaert F-X, Veyrat-Charvillon N (2010): Mutual information analysis: A comprehensive study. J Cryptol 24:269–291.

Baudewig J, Bittermann HJ, Paulus W, Frahm J (2001): Simultaneous EEG and functional MRI of epileptic activity: A case report. Clin Neurophysiol 112:1196–1200.

Berg AT, Berkovic SF, Brodie MJ, Buchhalter J, Cross JH, van Emde Boas W, Engel J, French J, Glauser TA, Mathern GW, Moshé SL, Nordli D, Plouin P, Scheffer IE (2010): Revised terminology and concepts for organization of seizures and epilepsies: Report of the ILAE commission on classification and terminology, 2005–2009. Epilepsia 51:676–685.

Bittar RG, Andermann F, Olivier A, Dubeau F, Dumoulin SO, Pike GB, Reutens DC (1999): Interictal spikes increase cerebral glucose metabolism and blood flow: A PET study. Epilepsia 40:170–178.

Chang C, Glover GH (2010): Time-frequency dynamics of resting-state brain connectivity measured with fMRI. NeuroImage 50: 81–98.

Delorme A, Makeig S (2004): EEGLAB: An open source toolbox for analysis of single-trial EEG dynamics including independent component analysis. J Neurosci Methods 134:9–21.

Eklund A, Nichols TE, Knutsson H (2016): Cluster failure: Why fMRI inferences for spatial extent have inflated false-positive rates. Proc Natl Acad Sci USA 113:7900–7905.

Fahoum F, Lopes R, Pittau F, Dubeau F, Gotman J (2012): Widespread epileptic networks in focal epilepsies: EEG-fMRI study. Epilepsia 53:1618–1627.

Fahoum F, Zelmann R, Tyvaert L, Dubeau F, Gotman J (2013): Epileptic discharges affect the default mode network—fMRI and intracerebral EEG evidence. PLoS One 8:e68038.

Federico P, Archer JS, Abbott DF, Jackson GD (2005): Cortical/subcortical BOLD changes associated with epileptic discharges An EEG-fMRI study at 3 T. Neurology 64:1125–1130.

Flanagan D, Abbott DF, Jackson GD (2009): How wrong can we be? The effect of inaccurate mark-up of EEG/fMRI studies in epilepsy. Clin Neurophysiol 120:1637–1647.

Flanagan D, Badawy RAB, Jackson GD (2014): EEG-fMRI in focal epilepsy: Local activation and regional networks. Clin Neurophysiol 125:21–31.

Glerean E, Salmi J, Lahnakoski JM, Jääskeläinen IP, Sams M (2012): Functional magnetic resonance imaging phase synchronization as a measure of dynamic functional connectivity. Brain Connect 2:91–101.

Gotman J (2008): Epileptic networks studied with EEG-fMRI. Epilepsia 49:42–51.

van Graan LA, Lemieux L, Chaudhary UJ (2015): Methods and utility of EEG-fMRI in epilepsy. Quant Imaging Med Surg 5: 300–312.

Grinsted A, Moore JC, Jevrejeva S (2004): Application of the cross wavelet transform and wavelet coherence to geophysical time series. Nonlinear Process Geophys 11:561–566.

Hipp JF, Hawellek DJ, Corbetta M, Siegel M, Engel AK (2012): Large-scale cortical correlation structure of spontaneous oscillatory activity. Nat Neurosci 15:884–890.

Iannotti GR, Grouiller F, Centeno M, Carmichael DW, Abela E, Wiest R, Korff C, Seeck M, Michel C, Pittau F, Vulliemoz S (2016): Epileptic networks are strongly connected with and without the effects of interictal discharges. Epilepsia 57:1086–1096.

Jackson GD, Pedersen M, Harvey AS (2017): How small can the epileptogenic region be? A case in point. Neurology 88:2017–2019.

Kilner JM, Mattout J, Henson R, Friston KJ (2005): Hemodynamic correlates of EEG: A heuristic. NeuroImage 28:280–286.

Laufs H, Hamandi K, Salek-Haddadi A, Kleinschmidt AK, Duncan JS, Lemieux L (2007): Temporal lobe interictal epileptic

discharges affect cerebral activity in "default mode" brain regions. Hum Brain Mapp 28:1023–1032.
Laufs H, Richardson MP, Salek-Haddadi A, Vollmar C, Duncan JS, Gale K, Lemieux L, Löscher W, Koepp MJ (2011): Converging PET and fMRI evidence for a common area involved in human focal epilepsies. Neurology 77:904–910.
Li X, Yao X, Fox J, Jefferys JG (2007): Interaction dynamics of neuronal oscillations analysed using wavelet transforms. J Neurosci Methods 160:178–185.
Liu X, Duyn JH (2013): Time-varying functional network information extracted from brief instances of spontaneous brain activity. Proc Natl Acad Sci USA 110:4392–4397.
Masterton RAJ, Abbott DF, Fleming SW, Jackson GD (2007): Measurement and reduction of motion and ballistocardiogram artefacts from simultaneous EEG and fMRI recordings. NeuroImage 37:202–211.
Masterton RAJ, Harvey AS, Archer JS, Lillywhite LM, Abbott DF, Scheffer IE, Jackson GD (2010): Focal epileptiform spikes do not show a canonical BOLD response in patients with benign rolandic epilepsy (BECTS). NeuroImage 51:252–260.
Masterton RAJ, Jackson GD, Abbott DF (2013): Mapping brain activity using event-related independent components analysis (eICA): Specific advantages for EEG-fMRI. NeuroImage 70:164–174.
Mulert C, Lemieux L, editors (2010): EEG—fMRI. Berlin, Heidelberg: Springer Berlin Heidelberg, http://link.springer.com/10.1007/978-3-540-87919-0
Noachtar S, Peters AS (2009): Semiology of epileptic seizures: A critical review. Epilepsy Behav EB 15:2–9.
Omidvarnia A, Azemi G, Colditz PB, Boashash B (2013): A time-frequency based approach for generalized phase synchrony assessment in nonstationary multivariate signals. Digit Signal Process 23:780–790.
Omidvarnia A, Azemi G, Boashash B, O'Toole JM, Colditz PB, Vanhatalo S (2014): Measuring time-varying information flow in scalp EEG signals: Orthogonalized partial directed coherence. IEEE Trans Biomed Eng 61:680–693.
Omidvarnia A, Pedersen M, Walz JM, Vaughan DN, Abbott DF, Jackson GD (2016): Dynamic regional phase synchrony (DRePS): An instantaneous measure of local fMRI connectivity within spatially clustered brain areas. Hum Brain Mapp 37:1970–1985.
Pedersen M, Omidvarnia A, Walz JM, Jackson GD (2015): Increased segregation of brain networks in focal epilepsy: An fMRI graph theory finding. NeuroImage Clin 8:536–542.
Pedersen M, Curwood EK, Vaughan DN, Omidvarnia A, Jackson GD (2016): Abnormal brain areas common to the focal epilepsies: Multivariate pattern analysis of fMRI. Brain Connect 6: 208–215.
Pedersen M, Omidvarnia A, Curwood EK, Walz JM, Rayner G, Jackson GD (2017): The dynamics of functional connectivity in neocortical focal epilepsy. NeuroImage Clin 15:209–214.
Ponce-Alvarez A, Deco G, Hagmann P, Romani GL, Mantini D, Corbetta M (2015): Resting-state temporal synchronization networks emerge from connectivity topology and heterogeneity. PLoS Comput Biol 11:e1004100.
Ponten SC, Bartolomei F, Stam CJ (2007): Small-world networks and epilepsy: Graph theoretical analysis of intracerebrally recorded mesial temporal lobe seizures. Clin Neurophysiol 118:918–927.
Power JD, Barnes KA, Snyder AZ, Schlaggar BL, Petersen SE (2012): Spurious but systematic correlations in functional connectivity MRI networks arise from subject motion. NeuroImage 59:2142–2154.
Salek-Haddadi A, Merschhemke M, Lemieux L, Fish DR (2002): Simultaneous EEG-correlated ictal fMRI. NeuroImage 16:32–40.
Salek-Haddadi A, Friston KJ, Lemieux L, Fish DR (2003): Studying spontaneous EEG activity with fMRI. Brain Res Rev 43: 110–133.
Schindler KA, Bialonski S, Horstmann M-T, Elger CE, Lehnertz K (2008): Evolving functional network properties and synchronizability during human epileptic seizures. Chaos Woodbury N 18:033119.
Tailby C, Masterton RAJ, Huang JY, Jackson GD, Abbott DF (2015): Resting state functional connectivity changes induced by prior brain state are not network specific. NeuroImage 106: 428–440.
Tao JX, Baldwin M, Hawes-Ebersole S, Ebersole JS (2007): Cortical Substrates of Scalp EEG Epileptiform Discharges. J Clin Neurophysiol 24:96–100.
Tokariev A, Palmu K, Lano A, Metsäranta M, Vanhatalo S (2012): Phase synchrony in the early preterm EEG: Development of methods for estimating synchrony in both oscillations and events. NeuroImage 60:1562–1573.
Torrence C, Compo GP (1998): A practical guide to wavelet analysis. Bull Am Meteorol Soc 79:61–78.
Villien M, Wey H-Y, Mandeville JB, Catana C, Polimeni JR, Sander CY, Zürcher NR, Chonde DB, Fowler JS, Rosen BR, Hooker JM (2014): Dynamic functional imaging of brain glucose utilization using fPET-FDG. NeuroImage 100:192–199.
Walz JM, Pedersen M, Omidvarnia A, Semmelroch M, Jackson GD (2017): Spatiotemporal mapping of epileptic spikes using simultaneous EEG-fMRI. Brain 140:998–1010.
Warren AEL, Harvey AS, Abbott DF, Vogrin SJ, Bailey C, Davidson A, Jackson GD, Archer JS (2017): Cognitive network reorganization following surgical control of seizures in Lennox-Gastaut syndrome. Epilepsia 58:e75–e81.
Yan C-G, Wang X-D, Zuo X-N, Zang Y-F (2016): DPABI: Data processing & analysis for (resting-state) brain imaging. Neuroinformatics 14:339–351.
Zalesky A, Fornito A, Cocchi L, Gollo LL, Breakspear M (2014): Time-resolved resting-state brain networks. Proc Natl Acad Sci USA 111:10341–10346.
Zang Y, Jiang T, Lu Y, He Y, Tian L (2004): Regional homogeneity approach to fMRI data analysis. NeuroImage 22:394–400.